D.P. LELEUX[1],✉
R. CLAPS[1]
W. CHEN[1]
F.K. TITTEL[1]
T.L. HARMAN[2]

Applications of Kalman filtering to real-time trace gas concentration measurements

[1] Rice Quantum Institute, Rice University, Houston, TX 77251-1892, USA
[2] Computer Engineering Department, University of Houston Clear Lake, Houston, TX 77058-1098, USA

ABSTRACT A Kalman filtering technique is applied to the simultaneous detection of NH_3 and CO_2 with a diode-laser-based sensor operating at $1.53\,\mu m$. This technique is developed for improving the sensitivity and precision of trace gas concentration levels based on direct overtone laser absorption spectroscopy in the presence of various sensor noise sources. Filter performance is demonstrated to be adaptive to real-time noise and data statistics. Additionally, filter operation is successfully performed with dynamic ranges differing by three orders of magnitude. Details of Kalman filter theory applied to the acquired spectroscopic data are discussed. The effectiveness of this technique is evaluated by performing NH_3 and CO_2 concentration measurements and utilizing it to monitor varying ammonia and carbon dioxide levels in a bioreactor for water reprocessing, located at the NASA–Johnson Space Center. Results indicate a sensitivity enhancement of six times, in terms of improved minimum detectable absorption by the gas sensor.

PACS 42.68.Ca; 42.62.Fi; 95.75.-z

1 Introduction

The primary focus of this work is the development of an adaptive filtering technique, known as Kalman filtering, to the sensitive, selective and real-time detection of NH_3 and CO_2 using a tunable diode-laser-based trace gas sensor [1–3]. The motivation for the application of this technique is the fact that these trace gas sensors have inherent laser, electrical and optical noise associated with them that manifests itself as short-term variations in gas concentration measurements. Examples of these real-time noise sources include thermal expansion or contraction of optical components, laser frequency drift and etalons. These fluctuations in concentration occur with every measurement, compared to true gas concentration variations that result from changes in the sample environment which evolve over the course of a series of measurements as reported in Sect. 4. This noise defines the minimum detection limit of the gas sensor, which can be characterized by calculating an Allan variance for the specific optical sensor configuration [4]. The Allan variance defines the optimal

✉ Fax: +1-713/348-5686, E-mail: leleux@rice.edu

averaging time for the gas analyzer, which minimizes the shot-to-shot variability of concentration measurements. Once this averaging time has been optimized, further detection sensitivity improvements can be achieved through the use of the Kalman filtering technique [5].

While numerous filtering techniques can be applied to post-processing of gas concentration measurements, only a few successful techniques have been identified that allow efficient on-line filtering of concentration measurements. One direct technique, which can be applied in real time, is simple averaging of the previous n measurements. The advantages of the Kalman filtering technique over simple averaging are three-fold:

- the Kalman filter incorporates all available measurements, regardless of their precision, and is not limited to a narrow window of n measurements to estimate the actual gas concentration;
- the Kalman filter (although the equations are more complex than an averaging technique) is computationally efficient because it is recursive and only requires two sets of information instead of n to be transferred from measurement to measurement for filter calculations; and
- the Kalman filter is adaptive and can adjust to changes in signal statistics and dynamic range during operation.

A comparison between a Kalman filter solution and a moving average technique is presented in Sect. 4.3. A Kalman filter combines all available measurement data, plus prior knowledge about the system and measuring devices, to produce an estimate of the actual concentration such that the error is minimized statistically. The use of this algorithm enables the filter to solve the Gauss' least-squares technique in real time with little or no delay in processing time.

The filtering algorithm was first developed in 1960 by Kalman [5] and applied to aerospace navigation problems. In 1993, Werle et al. employed adaptive filtering techniques to tunable diode-laser absorption spectroscopy (TDLAS) in the infrared molecular "fingerprint" region [6]. Subsequently, Kalman filtering applied to tunable diode-laser-based gas sensors was studied by Riris et al. in 1994 [7] and 1996 [8]. This paper describes the effective approach of applying Kalman filtering to real-time trace gas concentration measurements using diode-laser overtone spectroscopy.

In Sect. 2, the theoretical considerations of a Kalman filter will be described. Sect. 3 will explain sensor configuration and discuss data acquisition and processing. In Sect. 4, the results of the experiments will be analyzed and a comparison will be made between the Kalman filter and a moving average technique. The results will be summarized in Sect. 5.

2   Theoretical considerations

2.1   *Kalman filter model for trace gas concentration measurements*

In this section, we report on the application of Kalman filtering to address the problem of determining an optimal estimate of the true gas concentration, x_k, of a sample gas with a near-infrared diode-laser-based sensor in the presence of two sources of uncertainty (measurement noise introduced by the sensor, v_k, and true concentration variability, w_k). This scalar optimal estimation problem can be modeled by the linear stochastic difference equation [9, 10]:

$$x_{k+1} = x_k + w_k \,, \tag{1}$$

with measurements from the trace gas sensor, z_k, modeled as

$$z_k = x_k + v_k \,, \tag{2}$$

where the expected value, $E[w_k] = E[v_k] = 0$, and w_k and v_k are uncorrelated random variables with white noise variance of σ_w^2 and σ_v^2, respectively. The assumption of "whiteness" is valid for trace gas concentration measurements [9], since the noise variances are not correlated in time, i.e. knowing the noise variance at time x does not aid in predicting what its value will be at any other time. The variance σ_w^2 represents the true concentration variability while σ_v^2 represents the measurement noise introduced by the sensor.

$\hat{x}_k^-$ can be defined to be the *a priori* concentration estimate for a step k, with knowledge of the gas concentration prior to step k, and $\hat{x}_k$ to be the *a posteriori* concentration estimate for step k after the measurement value z_k is incorporated. Note that a hat above a variable such as $\hat{x}_k$ indicates an estimated or predicted quantity, and a superscript negative sign above a variable such as $\hat{x}_k^-$ indicates an *a priori* quantity. The *a priori* and *a posteriori* estimate errors can be defined as:

$$e_k^- \equiv x_k - \hat{x}_k^- \,, \tag{3}$$

and

$$e_k \equiv x_k - \hat{x}_k \,. \tag{4}$$

The *a priori* estimate error variance is then given by the expected value

$$P_k^- = E\left[e_k^- e_k^-\right] \,, \tag{5}$$

and the *a posteriori* estimate error variance is given by the expected value

$$P_k = E\left[e_k e_k\right] \,. \tag{6}$$

In deriving the Kalman filter equations, the objective is to find an equation that computes an *a posteriori* concentration estimate $\hat{x}_k$ as a linear combination of an *a priori* estimate $\hat{x}_k^-$

and a weighted difference between an actual concentration measurement z_k and a measurement prediction $\hat{x}_k^-$ as shown below:

$$\hat{x}_k = \hat{x}_k^- + K_k\left(z_k - \hat{x}_k^-\right) \,. \tag{7}$$

The difference $(z_k - \hat{x}_k^-)$ in (7) is called the measurement residual. The residual reflects the discrepancy between the predicted measurement $\hat{x}_k^-$ and the actual measurement z_k. A residual of zero means that the predicted and actual measurements are in complete agreement. The value of K_k in (7) is called the Kalman gain and is chosen to minimize the *a posteriori* error variance from (6). This minimization procedure can be accomplished by substituting (7) into (4), which defines e_k. Next, this result is substituted in (6), followed by performing the indicated expectations, taking the derivative of the result with respect to K_k, and setting this value equal to zero. Solving for K_k yields the definition of the Kalman gain, which minimizes (6), given by:

$$K_k = P_k^- \left(P_k^- + \sigma_v^2\right)^{-1} = \frac{P_k^-}{\left(P_k^- + \sigma_v^2\right)} \,. \tag{8}$$

From (8), it can be seen that the gain K_k weights the residual $(z_k - \hat{x}_k^-)$ more in (7) as the measurement error variance σ_v^2 approaches zero. In practical terms, this can be interpreted as a sensor that is reliable and provides measurements with low variability. Specifically, from (8),

$$\lim_{\sigma_v^2 \to 0} K_k = 1 \,.$$

However, as the measurement error variance σ_v^2 increases, the gain K_k weights the residual $(z_k - \hat{x}_k^-)$ less. Again, in practical terms, this can be interpreted as a sensor that provides measurements with significant variability. In the limit, as σ_v^2 approaches infinity, from (8),

$$\lim_{\sigma_v^2 \to \infty} K_k = 0 \,.$$

Another way of interpreting the weighting by K_k is that as the measurement error variance σ_v^2 approaches zero, the actual measurement z_k is "trusted" more because the sensor becomes more reliable and the predicted measurement $\hat{x}_k^-$ is trusted less. However, as the measurement error variance σ_v^2 increases, the actual measurement z_k is trusted less because the sensor is considered less reliable in terms of variability, while the predicted measurement $\hat{x}_k^-$ is trusted more.

By substituting (8) into (7) and using (3) through (6) to solve for P_k, the solution provides the *a posteriori* estimate error variance as:

$$P_k = (1 - K_k)\, P_k^- \,. \tag{9}$$

With (8) and (9), the complete *a posteriori* estimate and error variance are defined as a function of the weighting factor K_k that is conditioned based on both the previous uncertainty of the estimate and the uncertainty of the measuring device.

2.2 *The Kalman filter algorithm*

The Kalman filter estimates the gas concentration by using a form of feedback control. The filter estimates the concentration at some given time and then obtains feedback in the form of measurements possessing a noise component. As such, the Kalman filter equations fall into two groups: time update equations and measurement update equations. The time update equations are responsible for projecting forward in time current concentration and error variance estimates to obtain *a priori* estimates for the next time step. Table 1 shows the equations used in the time update portion of the algorithm.

If the gas concentration is determined by a process that can be modeled directly or inferred (e.g. from temperature), this information can be used to obtain a better predictive capability instead of assuming that the next concentration will be equal to the previous concentration plus some noise, as in (1). If a control input can be modeled by a variable, u_k (e.g. the gas concentration is determined by the temperature in a reaction chamber at a chemical processing plant), then the time update (10) can be modified to include this information, as shown in (12).

The measurement update equations are responsible for the feedback, i.e. for incorporating a new measurement into the *a priori* concentration estimate to obtain an improved *a posteriori* estimate, and are given in Table 2.

The time update equations act then as predictor equations, while the measurement update equations act as corrector equations. The final estimation algorithm is a predictor–corrector algorithm for solving the least-squares method in real time as shown in Fig. 1.

The first step in the sequence involves selecting initial *a priori* values for the concentration estimate, $\hat{x}_k^-$, and the error variance, P_k^-. The selection of these quantities is not critical, since the filter will converge to an appropriate value. However, they should be chosen to be within the dynamic range of the expected gas concentrations and errors to speed convergence. The next step involves taking a measurement update from the sensor by first computing the Kalman gain, K_k, using (13). Subsequently, the sensor performs a concentration measurement to obtain z_k. This is followed by calculating an *a posteriori* concentration estimate using (14), and the final step is to obtain an *a posteriori* error variance estimate from (15).

Once *a posteriori* estimates of the concentration and variance are obtained, a time update is processed using (10) and (11), or (10) and (12) if a control input is modeled. This step
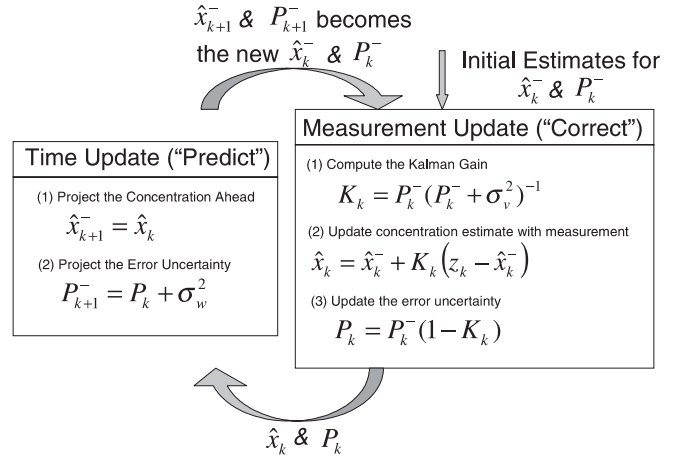

FIGURE 1   Complete Kalman filter cycle. The time update projects the current concentration estimate ahead in time. The measurement update adjusts the projected concentration estimate by an actual measurement at that time. Note: σ_v^2 and σ_w^2 are constants

projects the concentration and variance estimates from time step k to step $k+1$.

After each time and measurement update pair, the process is repeated with the previous *a posteriori* estimates used to project or predict the new *a priori* estimates. This recursive nature is one of the appealing features of the Kalman filter, because it recursively conditions the current concentration estimate on all of the past measurements. Furthermore, the selection of σ_w^2 and σ_v^2 is one of the central features in tuning the Kalman filter to provide the optimum sensor performance, as discussed in Sect. 4.

3 Experimental details

3.1 *Diode-laser-based gas sensor*

The diode-laser-based sensor shown in Fig. 2 for gas detection and quantification using vibrational overtone spectroscopy at $1.53\,\mu m$ was used to investigate the Kalman
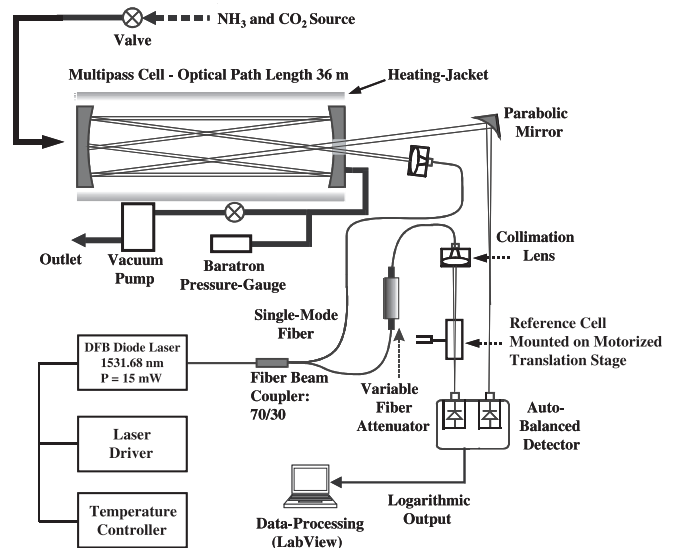
$$\hat{x}_{k+1}^- = \hat{x}_k \tag{10}$$
$$P_{k+1}^- = P_k + \sigma_w^2 \tag{11}$$
$$\hat{x}_{k+1}^- = \hat{x}_k + u_k \tag{12}$$

TABLE 1   Kalman filter time update equations

$$K_k = P_k^-(P_k^- + \sigma_v^2)^{-1} \tag{13}$$
$$\hat{x}_k = \hat{x}_k^- + K_k(z_k - \hat{x}_k^-) \tag{14}$$
$$P_k = (1 - K_k)P_k^- \tag{15}$$

TABLE 2   Kalman filter measurement update equations

FIGURE 2   Diode-laser-based trace gas sensor configuration for continuous NH_3 and CO_2 concentration measurements at $1.53\,\mu m$

	Linestrength		Frequency	Wavelength	Ref.
	cm^{-1}/(molecule/cm^2)	cm^{-2} atm^{-1} (@ 296 K)	cm^{-1}	nm	
A	2.33×10^{-21}	0.0578	6528.76	1531.68	[11]
B	1.24×10^{-21}	0.0307	6528.89	1531.65	[11]
C	5.19×10^{-25}	1.29×10^{-5}	6528.895	1532.65	[12]

TABLE 3   NH$_3$ and CO$_2$ overtone absorption lines used in this work

filtering technique. This sensor has been described in detail previously [1–3]. An ammonia (or any other gas) concentration measurement for narrow-linewidth radiation sources is obtained by using the Beer–Lambert absorption law, which relates the intensity of light entering into an absorption medium, I_0, to the transmitted intensity, I, as follows:

$$\frac{I}{I_0} = \exp\left(-S_\nu \phi_\nu P \chi_j l\right) \qquad (16)$$

where S_ν is the temperature-dependent absorption line strength for a specific transition denoted by $\nu\,[\mathrm{cm}^{-2}\mathrm{atm}^{-1}]$, ϕ_ν is the line shape function (cm), χ_j is the fractional concentration of the species j, P is pressure (atm), and l is the optical path length through the medium (cm).

Table 3 depicts the three NH$_3$ and CO$_2$ absorption lines that are used in this work. Lines A and B are the two ammonia lines used: A is an isolated line useful for measuring ammonia concentrations while line B overlaps with line C, which is the $(00001) \leftarrow (30011)$, $R(36)$, overtone transition of CO$_2$. These three lines are accessible using a 1.53 μm telecommunications diode-laser.

The sensor consists of three main components: a single-frequency, fiber pig-tailed, tunable, distributed feedback (DFB) diode-laser (NTT-NEL Electronics), a multi-pass absorption cell and a dual-beam auto-balanced InGaAs detector (Nirvana 2017, New Focus, Inc). The laser diode is driven by a compact current supply (MPL-250, Wavelength Electronics) with ripple noise < 1 μA, so that the frequency fluctuations of the laser line due to current noise are negligible (< 1 MHz). The current supply is scanned at 20 Hz about an average current of 67 mA with a saw-tooth ramp function. The laser temperature was controlled to within 0.003 °C, close to 32 °C, by a current module (HTC-1500, Wavelength Electronics). The scan range of the laser under these conditions was 0.3 cm^{-1}, which allowed all the spectral lines of interest to be accessed on every scan.

The fiber-pigtailed DFB laser diode delivers 15 mW at 1531.7 nm with a specified linewidth of < 10 MHz. The fiber was fusion-spliced to a 70/30% directional coupler with an insertion loss of less than 2%. The 70% power arm of the directional coupler was sent to the multi-pass cell, using a lens ($f = 7$ mm, 0.5 NA) mounted in a precision holder with 5 degrees of freedom (Optics For Research) to set the beam waist at the midpoint of the multi-pass cell. The 30% power arm was used as the reference beam for the balancing detector. Such an integrated laser and optical fiber configuration delivers 10 mW of laser light at the input of the multi-pass cell. The output power of the beam obtained from the cell after 182 passes was 200 μW, resulting in a throughput efficiency of 2.0% (a factor of 10 better than for the cell described in [1]). The output beam from the cell is focused on the signal and reference photodiodes of the dual beam detector by a gold-coated, parabolic mirror of 2.54 cm diam-

eter (f-number $= 2$) and a lens ($f = 7$ mm, 0.5 NA) mounted on a precision holder, respectively. Since the reference beam power (P_{ref}) was much greater than the power of the signal beam coming from the cell (P_{signal}), it was attenuated using a variable fiber attenuator. For optimum performance of the auto-balanced detector, the reference power was set as $P_{\mathrm{ref}} = 2.2 \times P_{\mathrm{signal}}$, at the center frequency of the laser scan. This in turn reduces the attenuation level required at the reference input of the detector to ~ 3 dB, a range where the operation of the fiber attenuator is reliable and free of fringing effects.

All elements, except the input and output of the multi-pass cell, are coupled to optical fibers in order to make the system suitable for field applications. A two-stage, micro-mechanical diaphragm pump mounted next to the multi-pass cell provides a continuous flow of sample gas at a rate that is controlled by two needle valves at the input and output of the multi-pass cell, which has a volume of 0.3 liters. For these experiments, an optimal flow rate of about 100 sccm allows for a fast response of the instrument to true concentration changes, while keeping the concentration rates of the gas sample stable. The multi-pass cell was heated to a temperature of 40 °C to minimize ammonia adsorption on its glass walls. All the measurements presented here were obtained with the sample gas inside the multi-pass cell at a fixed pressure of 100 Torr. For the measurements, a cylinder containing certified 99.99% pure CO$_2$ (Scott Specialty Gases, Inc.) was connected in parallel with an ammonia gas-dilution system [1]. The ammonia sample was obtained by diluting a certified, 100 ppm NH$_3$ mixture in N$_2$ (Matheson), with a pure N$_2$ sample. The fraction of NH$_3$ introduced in the mixture was controlled to within ± 0.2 ppm by using a mass flow controller [MKS Instruments, Inc.], whereas the CO$_2$ concentration was regulated to within ± 1000 ppm by adjusting the outlet pressure of the cylinder regulator.

Other modifications were introduced in order to improve the operation of the instrument that was reported in [1–3]: A pure ammonia cell (1 Torr) was used for real-time frequency calibration. This cell was attached to a motorized translational stage (New Focus, Model No. 8892) that inserts the reference cell periodically into the optical path of the signal beam. This is accomplished using a software-generated TTL pulse from the data acquisition routine. To automatically account for operational fluctuations in the gas handling system, pressure and temperature are measured in real time and their values are updated in the data analysis routine for each concentration measurement. By implementing these modifications, the system is now a stand-alone instrument that can be used for on-line remote operation over extended periods of time, monitoring the concentration of trace gases such as NH$_3$ and CO$_2$. This is particularly useful for demonstrating the capabilities of the Kalman filtering technique, which

provides an optimal estimate of the true gas concentration continuously.

3.2 *Data processing: acquisition and analysis*

A laptop PC running LabView 5.0 software was used for data acquisition and processing. With the photodetector operating in auto-balance mode, 500 spectral scans were averaged for each single concentration measurement. The total data collection time, averaging and processing to obtain a single concentration measurement was less than 30 s. For convenience, the sensor was configured to take measurements every minute in order to correlate ammonia measurements to external daily events. The capability to remotely monitor the sensor performance and concentration data was implemented by using "PC Anywhere" software.

The real-time fitting routine implemented in LabView has been reported elsewhere [13], and only minor software modifications were required for this work. Initially a direct transmission spectrum from the logarithmic output of the Nirvana detector, operating in auto-balance mode, is obtained and a 3rd order polynomial is fitted to the baseline of the absorption scan. If a voltage, $V^*(\nu)$, is assigned to the baseline values, and the logarithmic signal values are assigned a voltage $V(\nu)$, then the corresponding optical transmission for the given frequency value, $T(\nu)$, in percent, is given by [14]:

$$T(\nu) = 100 \frac{e^{-\frac{A}{T}V^*(\nu)} + 1}{e^{-\frac{A}{T}V(\nu)} + 1} \qquad (17)$$

where T is the temperature of the photodetector (taken to be 300 K), and A is a constant determined by the gain in the amplifier circuit of the detector ($A = 273$ K/V). This procedure provides a balanced transmission spectrum and simultaneously corrects for the baseline of the absorption signal. To this spectrum (after dividing by 100 and taking the natural logarithm), an absorption line-shape function is fitted to obtain the gas concentration as described below. The convenience of this procedure is that only one detection channel is needed in this configuration to account for both the signal and reference outputs in the photo-detector.

The fit employs a non-linear, least-squares Levenberg–Marquardt algorithm and uses a given absorption profile to fit the data. Since the pressure regime of operation (100 Torr) lies between the predominantly Doppler and pressure-broadened regimes, a triple Voigt profile with fixed pressure broadening and Doppler width was used. Typical absorption spectra obtained were fitted to a third-order polynomial and three Voigt profiles [15, 16], with a linewidth of $0.027\,\text{cm}^{-1}$ and a pressure broadening contribution of $0.020\,\text{cm}^{-1}$. Small pressure fluctuations in the system of ± 1 Torr are accounted for in real time by the data collection software. Therefore, the linewidth of the ammonia and carbon dioxide absorption peaks was expected to fluctuate by less than $\pm 0.001\,\text{cm}^{-1}$ [17–19]. This introduces an error for the ammonia and carbon dioxide concentration measurements in the fitting routine of 2%. The residual of the Voigt fit in typical 2.8 ppm NH_3 spectra (peak absorption of 0.14%) yields an uncertainty level for a single measurement (with 500 averages) of $\pm 0.01\%$ – absorption – (note that $100 \times \ln(I/I_0)$ is equivalent to % absorption for

small absorptions). The rms uncertainty level is then 0.014% absorption and a peak absorption and corresponds to 2.8 ppm of NH_3. This is the minimum concentration that can be measured reliably with the reported gas sensor design, without any further data filtering. Optical fringes from interference effects introduced by the multi-pass cell limit the sensitivity and are the primary source of uncertainty in the ammonia and carbon dioxide concentration values reported.

4 Experimental results and discussion

4.1 *Kalman filter parameters and tuning*

The development of a Kalman filter for real-time measurements that may vary by an order of magnitude requires the selection of appropriate values for σ_w^2 (true concentration variability) and σ_v^2 (measurement noise introduced by the sensor). Both of these variances represent the concentration variability from one measurement to the next. For instance, σ_w^2 represents how much the true concentration would be expected to vary from one measurement to the next, and σ_v^2 represents how much noise the sensor may be expected to introduce into the measured concentration from one measurement to the next.

The σ_v^2, value may be measured while operating the sensor at a constant gas concentration to determine the variance of the measured concentrations. This value may then be used as a constant in a real-time filter operation. However, such a calculation is not valid over all dynamic ranges, since the concentration variability changes in direct proportion to the concentration range. This is shown in Fig. 3, where the vari-
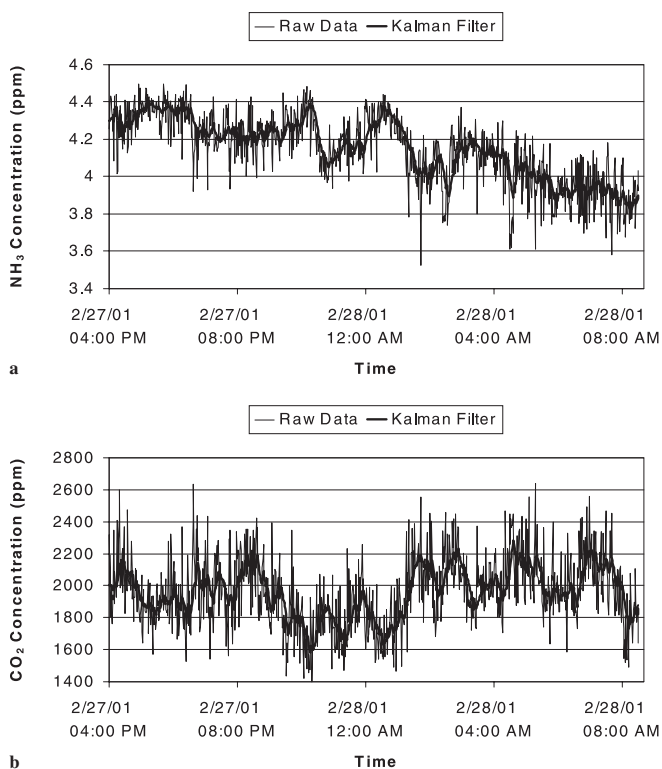

a

b

FIGURE 3 Simultaneous NH_3 (**a**) and CO_2 (**b**) concentration measurements for a 16-h period. Kalman filter results are indicated by a *thick bold line* while raw data measurements appear as *thin lines* depicting system noise

ability of the ammonia is 0.1 ppm for values of ~ 4 ppm, but the variability of the carbon dioxide is about 158 ppm for values of ~ 2000 ppm. Under any given experimental circumstances, once the measurement system has reached equilibrium, then:

$$\lim_{t \to \infty} \frac{\sigma_v^2}{\sigma_w^2} = \varrho \,, \tag{18}$$

where t is the time the system has been operating and ϱ is a constant. Therefore, if the true concentration changes by orders of magnitude, the variance will also change by orders of magnitude. The measurement uncertainty may also change as a result of different operating conditions resulting from temperature or humidity variations as well as aging of the sensor. These effects can be particularly obvious in the case of field experiments where controlling the environmental conditions for the sensor is difficult. Recalculation of the variance of a set of measurements periodically during the operation of the sensor and using that variance to recalculate the values of σ_v^2 and σ_w^2 while subsequently using the recalculated values for filter operation can mitigate the effect of large range changes.

Since variability scales roughly linearly as true concentration changes, this observation can be used to develop a scheme for automating the selection of σ_v^2 and σ_w^2. This method involves first applying a small window (e.g. the previous 10 raw measurements) to calculate the sample concentration variance. This value is then used as the choice for σ_v^2. Since the measurement variability (σ_v^2) scales linearly as true concentration changes (σ_w^2), the following steady-state condition must hold true according to (18):

$$\frac{\sigma_v^2}{\sigma_w^2} = \varrho \,, \tag{19}$$

where ϱ is a constant. σ_w^2 can then be calculated by dividing σ_v^2 by ϱ. The value ϱ can then be used as a tuning parameter to control how rapidly the filter will respond to measurement changes in calculating the Kalman filter output. The larger the ratio, the longer it will take for radical changes in measured concentrations to be incorporated into the filter output. The smaller the ratio, the more susceptible the filter will be to accept large changes in measured concentrations. In other words, the higher frequency components will have less affect on the filter output as ϱ is increased. This method was used for filter calculations reported in this work. The selection of a value for ϱ was made empirically as described in Sect. 4.2. The use of the variance ratio technique allows for a completely automated selection process for σ_v^2 and σ_w^2 assuming a constant value for ϱ. Note that the value of ϱ depends on the specific circumstances of the concentration measurement, which includes both the sensor and the system that is being measured. Therefore ϱ is not an intrinsic property of the gas sensor.

4.2 *Kalman filter results and sensor performance*

The Kalman filter using the variance ratio technique was applied during the operation of the trace gas sensor

for a period of approximately 16 h. For this period, 1000 simultaneous concentration measurements of NH_3 and CO_2 were acquired. The results of such a test are shown in Fig. 3. Ammonia and carbon dioxide concentrations are shown in Fig. 3a and 3b, respectively. A thin line indicates raw data measurements, while Kalman filter calculations are designated by thick lines. As expected, the raw data is significantly noisier than the filtered data. The detection sensitivity for the NH_3 was 0.12 ppm without Kalman filtering. After applying Kalman filtering, the data variability was reduced to a concentration uncertainty of 0.02 ppm. By dividing the uncertainty before the Kalman filter was applied by the uncertainty after employing the Kalman filter, a detection sensitivity improvement by a factor of six was indicated. Detection sensitivity improvement is equal to the ratio of the measurement standard deviation (σ) without a Kalman filter to the measurement stan-
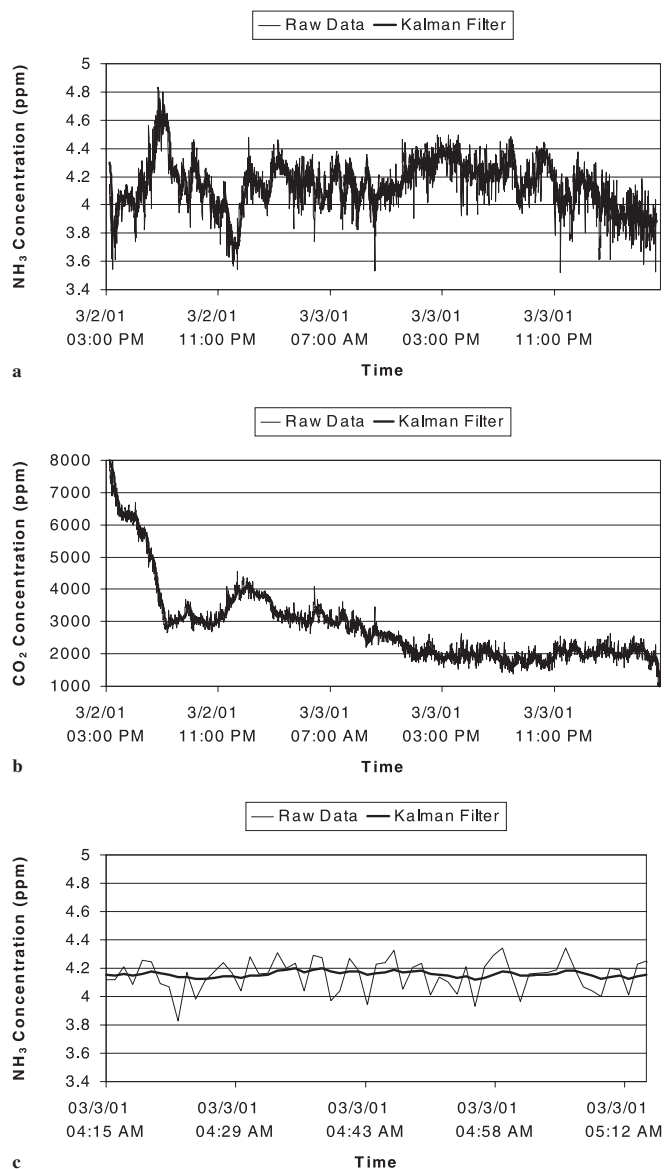

FIGURE 4 NH_3 and CO_2 concentration measurements for a 39-h data collection run indicating good filter performance for a factor of 4 change in the CO_2 dynamic range (**a** and **b**); a typical 1-h zoom-in of the NH_3 concentration data with ϱ set to 50 is depicted in **c**

dard deviation with a Kalman filter. An improvement by a factor of two was observed for CO_2 measurements. The Kalman filter output clearly follows true concentration changes modeled in terms of σ_w^2 while ignoring the variability caused by sensor noise and modeled by σ_v^2. A value of 50 was used for ϱ.

In a further evaluation test, the performance of the Kalman filter was investigated over a significant dynamic range by allowing the CO_2 concentration to change by a factor of 4, from 8000 ppm to 2000 ppm. The NH_3 concentration was held constant at 4 ppm. This test was allowed to run for approximately 39 h. During this time, 2500 concentration measurements were obtained. The result of this experiment is shown in Fig. 4. As in the previous test, ammonia and carbon dioxide concentrations are shown in Fig. 4a and 4b. The detection sensitivity for the NH_3 measurement was 0.12 ppm without the Kalman filtering. After applying the Kalman filtering, the data variability was reduced to a concentration uncertainty of 0.02 ppm. This indicates a detection sensitivity improvement by a factor of six. Similarly, an improvement by a factor of 2.5 was observed for CO_2 measurements. Again, the Kalman filter output followed true concentration changes over a large dynamic range and the variability caused by sensor noise is minimized. As previously, a value of 50 was used for ϱ. Figure 4c, a 1-h zoom-in on Fig. 4a data, clearly illustrates the effectiveness of applying the Kalman filter to improve the detection sensitivity.

A subsequent experiment involved performing several data collection runs for different values of ϱ in order to ascertain the effects of varying this parameter. A result of this experiment, shown in Fig. 5, indicates that as ϱ increases, the filter solution lags behind the true concentration changes. A ϱ value of 250 was used in Fig. 5. This effect is one of the limitations of the variance ratio technique. If ϱ is made too large, the filter solution will lag behind true changes in concentration. As ϱ is increased, this effect becomes more pronounced. Data collection was performed using five values for ϱ including 50, 100, 150, 200, and 250. The best overall sensor performance was observed with a value of 50, although reasonable filter performance was observed with all of these values.

A field test of the sensor was performed at the NASA Johnson Space Center in Houston, TX as described in [1–3]. The measurement involved the monitoring of a packed-bed biological water processor (BWP) that is part of a NASA water recovery system (WRS). This system produces potable water from waste water using aerobic and anaerobic microbial processes. Two of the byproducts of the chemical reaction in the bioreactor are ammonia and carbon dioxide. During one data collection run, the Kalman filter was operated in real time as data was being collected. Figure 6 shows an excerpt of the CO_2 data collected together with the corresponding Kalman filter results processed after the run.

In a subsequent laboratory and field test on the same BWP system described above, a pulsed, thermoelectrically cooled, single-frequency quantum cascade laser was used to access two NH_3 absorption lines of the fundamental ν_2 band at 10 microns [20]. Comparable results to the overtone data were obtained by measuring changes in ammonia concentration over a 15-h time period. The NH_3 concentration was varied from 10 ppm to 40 ppm. The detec-
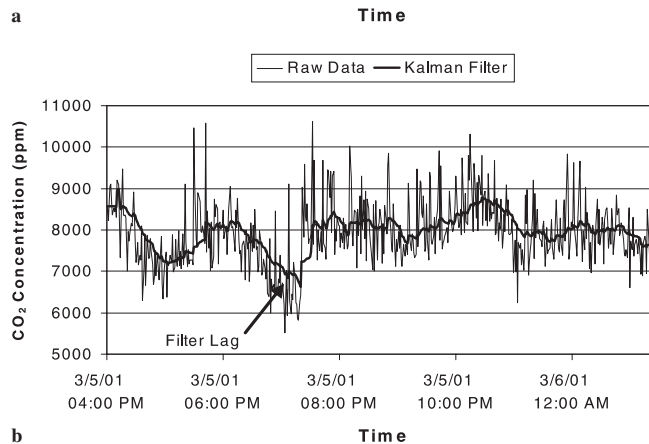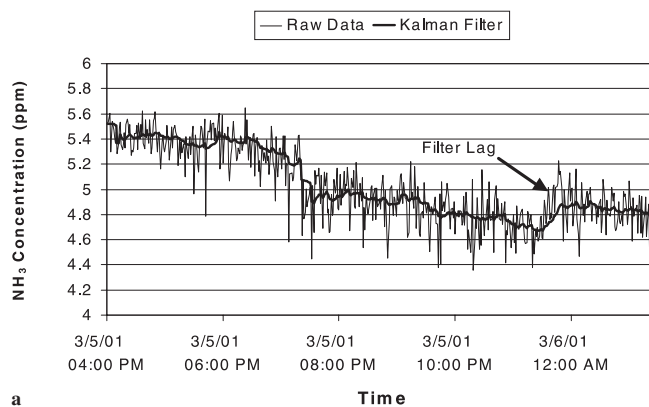
FIGURE 5 NH_3 (**a**) and CO_2 (**b**) concentration measurements for a 9-h time series with ϱ set to 250, indicating a filter delay in accepting large changes to the measured data
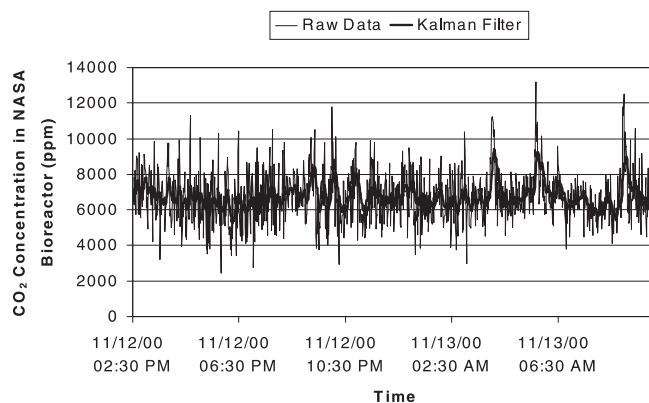
FIGURE 6 CO_2 concentration measurements and Kalman filter results from a biological water processor located at the NASA Johnson Space Center, Houston, TX. The Kalman filter data depicted was applied to the concentration measurements after its acquisition

tion sensitivity was 0.3 ppm without Kalman filtering and improved the precision to 0.04 ppm after applying Kalman filtering to the NH_3 concentration data. This indicates an enhancement of the minimum detection sensitivity by a factor of 7.5.

4.3   *Comparison of Kalman filter results to a moving average*

As discussed in the introduction, there are a number of advantages of the Kalman filter over the moving average technique. Using the raw CO_2 measurement data in
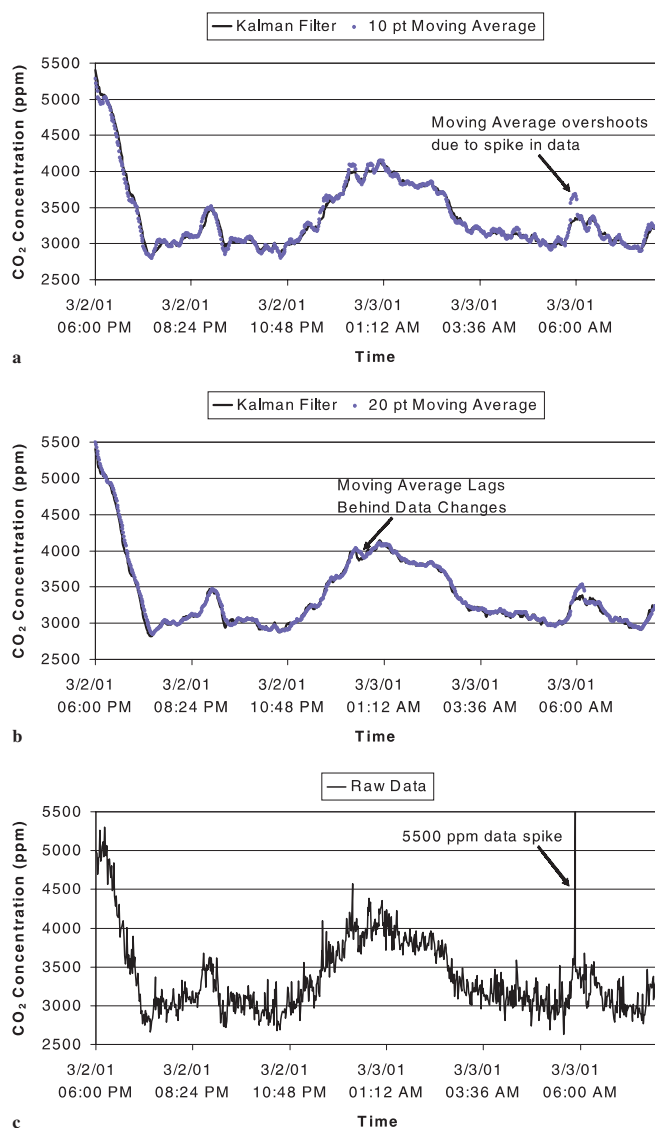
FIGURE 7 Time series of CO_2 measurements showing a comparison between a Kalman filter solution and two moving average solutions. *Inset* **a** shows a Kalman filter solution versus a 10-point moving average while *inset* **b** displays the same Kalman filter solution against a 20-point moving average. The final *inset* **c** displays the raw data used in both the Kalman filter as well as the moving average solutions

Fig. 7c, a Kalman filter solution was calculated as well as a 10- and 20-point moving average. These results are shown in Figs. 7a and 7b respectively. The results show similar behavior between the Kalman filter and the moving average; however, the advantages of the Kalman filter show up in two key ways.

The first place the Kalman filter shows superiority to the moving average is when abnormally large spikes are generated by the sensor. For instance at 3/3/01 5 : 52 in Fig. 7c, a spike of 5500 ppm was generated. Observing surrounding data, a "real" concentration of 5500 ppm seems highly unlikely. The Kalman filter is conditioned on all previous data, so it is unaffected by this spike. The moving average technique, however, is significantly impacted by the spike and takes several measurements before it returns to normal.

One way of dealing with these spikes is to increase the number of points in the moving average. The 20-point moving average shows a diminished impact of the spike; however, its overall performance is degraded. If the number of points in the moving average window is made too large, a "lagging" effect will be observed causing key features to be missed, e.g. at 3/3/01 0 : 39. This feature is similar to the behavior of an un-tuned Kalman filter. However, once ϱ is optimized, both of the problems identified above are solved, as described in Sect. 4.1. This is one of the key advantages of the Kalman filter, which is its adaptivity to changing data statistics.

5   Conclusions and outlook

In summary, an automated trace gas sensor that required no operator intervention during data collection was demonstrated. The use of a Kalman filter significantly improved the detection sensitivity of the diode-laser-based gas sensor by a factor of two to six when using $1.5\,\mu m$ overtone absorption lines and by a factor of 7.5 when performing ammonia concentration measurements at $10\,\mu m$ with fundamental absorption lines, by determining on-line an optimum estimate of the true concentration to reduce the variability. Both the theory and implementation of a practical Kalman filter were discussed and limitations of certain aspects of this technique were analyzed. The operation of the Kalman filter with two different dynamic ranges corresponding to the two gases used was successfully demonstrated. Detection sensitivity factor improvements of six and two were observed at concentration levels of 4 and 1500 ppm for NH_3 and CO_2, respectively.

Potential applications of the Kalman filter technique include its use in environmental, medical and industrial process control. For example, identification and modeling of gas concentrations in chemical manufacturing processes will provide measurable indicators or indirect control of the gas concentrations. This could be modeled in terms of a control input u_k as discussed in Sect. 2.2. This modeling can improve the predictive capability and accuracy of the filter. This modeling was not included in the experiments presented in this paper, since no measurable indicators were available for improving the predictive capability of the filter.

One limitation of the Kalman filtering technique as presented in this work is the fact that it must operate on concentration values after a data processing algorithm has reduced them. A potentially more accurate method would be to operate the filter directly on the absorption profile output of the detector prior to the non-linear least-squares fitting routine as discussed in [1]. Significant variations in absorption profiles often cause problems with applied non-linear least-squares routines even after averaging, which can add additional noise to the sensor output above the hardware noise due to white noise variance of σ_v^2.

REFERENCES

1 R. Claps, F.V. Englich, D. Leleux, D. Richter, F.K. Tittel, R.F. Curl: Appl. Opt. **40**, 4387 (2001)
2 M.E. Webber, R. Claps, F.V. Englich, F.K. Tittel, J.B. Jeffries, R.K. Hanson: Appl. Opt. **40**, 4395 (2001)
3 R. Claps, D. Leleux, F.V. Englich, F.K. Tittel, M.E. Webber, J. Jeffries, R.K. Hanson, J.C. Graf, L.M. Vega: Infrared overtone spectroscopy measurements of ammonia and carbon dioxide in the effluent of a biological water processor. In: Proc. 31st Int. Conf. on Environmental Systems (ICES), Society of Automotive Engineers, Inc., Orlando, FL July 9–12, 2001
4 P. Werle, R. Mücke, F. Slemr: Appl. Phys. B **57**, 131 (1993)
5 R.E. Kalman: Trans. ASME, J. Basic Eng. **82**, 35 (1960)
6 P. Werle, B. Scheumann, J. Schandl: Optical Engineering **33**, 3093 (1993)
7 H. Riris, C.B. Carlisle, R.E. Warren: Appl. Opt. **33**, 5506 (1994)
8 H. Riris, C.B. Carlisle, R.E. Warren, D.E. Cooper, R.U. Martinelli, R.J. Menna, P.K. York, D.Z. Garbuzov, H. Lee, J.H. Abeles, N. Morris, J.C. Connolly, S.Y. Narayan: Spectrochimica Acta A **52**, 843 (1996)
9 C.W. Helstrom: *Probability and Stochastic Processes for Engineers*, 2nd edn. (Macmillan, New York 1991)
10 P. Maybeck: *Stochastic Models, Estimation, and Control*, Vol. 1 (Academic Press, New York 1979)
11 M.E. Webber, D.S. Baer, R. Hanson: Appl. Opt. **40**, 2031 (2001)
12 L.S. Rothmann, C.P. Rinsland, A. Goldman, S.T. Massie, D.P. Edwards, J.Y. Mandin, J. Schroeder, A. McCann, R.R. Gamache, R.B. Wattsin, K. Yoshino, K.V. Chance, K.W. Juck, L.R. Brown, V. Nemtchechin, P. Varanasi: J. Quant Spectrosc. Radiat. Transfer **60**, 665 (1998)
13 D.G. Lancaster, D. Richter, R.F. Curl, F.K. Tittel: Appl. Phys. B **67**, 339 (1998)
14 K.L. Haller, P.C.D. Hobbs: Proc. SPIE **1435**, 298 (1991)
15 E.E. Whiting: J. Quant. Spectrosc. Radiat. Transfer, **8**, 1379 (1968)
16 D.J. Brassington: *Tunable diode laser absorption spectroscopy for the measurement of atmospheric species*. In: *Spectroscopy in Environmental Science*, ed. by R.J.H. Clark, R.E. Hester (Wiley, New York 1995) pp. 85–147
17 G. Modugno, C. Corsi: Infrared Phys. Technol. **40**, 93 (1999)
18 L. Lundsberg-Nielsen, F. Hegelund, F.M. Nicolaisen: J. Molec. Spectrosc. **162**, 230 (1993)
19 C.H. Townes, A.L. Schawlow: *Microwave Spectroscopy* (McGraw-Hill, New York 1955) p. 364, Table 13.4
20 A. Kosterev, R.F. Curl, F.K. Tittel, R. Köhler, C. Gmachl, F. Capasso, D. Sivco, A. Cho: Appl. Opt., to appear January 20, 2002